


RESEARCH

Open Access



M-type pyruvate kinase 2 (PKM2) tetramerization alleviates the progression of right ventricle failure by regulating oxidative stress and mitochondrial dynamics

Lizhe Guo¹, Lu Wang¹, Gang Qin¹, Junjie Zhang¹, Jin Peng¹, Longyan Li¹, Xiang Chen¹, Dandan Wang^{2,3}, Jian Qiu^{2,3,4*} and E. Wang^{1,3*} 

Abstract

Background Right ventricle failure (RVF) is a progressive heart disease that has yet to be fully understood at the molecular level. Elevated M-type pyruvate kinase 2 (PKM2) tetramerization alleviates heart failure, but detailed molecular mechanisms remain unclear.

Objective We observed changes in PKM2 tetramerization levels during the progression of right heart failure and in vitro cardiomyocyte hypertrophy and explored the causal relationship between altered PKM2 tetramerization and the imbalance of redox homeostasis in cardiomyocytes, as well as its underlying mechanisms. Ultimately, our goal was to propose rational intervention strategies for the treatment of RVF.

Method We established RVF in Sprague Dawley (SD) rats by intraperitoneal injection of monocrotaline (MCT). The pulmonary artery pressure and right heart function of rats were assessed using transthoracic echocardiography combined with right heart catheterization. TEPP-46 was used both in vivo and in vitro to promote PKM2 tetramerization.

Results We observed that oxidative stress and mitochondrial disorganization were associated with increased apoptosis in the right ventricular tissue of RVF rats. Quantitative proteomics revealed that PKM2 was upregulated during RVF and negatively correlated with the cardiac function. Facilitating PKM2 tetramerization promoted mitochondrial network formation and alleviated oxidative stress and apoptosis during cardiomyocyte hypertrophy. Moreover, enhancing PKM2 tetramer formation improved cardiac mitochondrial morphology, mitigated oxidative stress and alleviated heart failure.

Conclusion Disruption of PKM2 tetramerization contributed to RVF by inducing mitochondrial fragmentation, accumulating ROS, and finally promoted the progression of cardiomyocyte apoptosis. Facilitating PKM2 tetramerization holds potential as a promising therapeutic approach for RVF.

Keywords Pulmonary arterial hypertension, Right ventricular failure, PKM2 tetramerization, Mitochondrial dynamics, Myocardial apoptosis

*Correspondence:

Jian Qiu

qiuqjian@sklmg.edu.cn

E. Wang

ewang324@csu.edu.cn

Full list of author information is available at the end of the article



© The Author(s) 2023. **Open Access** This article is licensed under a Creative Commons Attribution 4.0 International License, which permits use, sharing, adaptation, distribution and reproduction in any medium or format, as long as you give appropriate credit to the original author(s) and the source, provide a link to the Creative Commons licence, and indicate if changes were made. The images or other third party material in this article are included in the article's Creative Commons licence, unless indicated otherwise in a credit line to the material. If material is not included in the article's Creative Commons licence and your intended use is not permitted by statutory regulation or exceeds the permitted use, you will need to obtain permission directly from the copyright holder. To view a copy of this licence, visit <http://creativecommons.org/licenses/by/4.0/>. The Creative Commons Public Domain Dedication waiver (<http://creativecommons.org/publicdomain/zero/1.0/>) applies to the data made available in this article, unless otherwise stated in a credit line to the data.

Introduction

Pulmonary arterial hypertension (PAH) describes patients with an average pulmonary artery pressure of >20 mmHg, characterized by a progressive increase in pulmonary vascular resistance, eventually leading to right ventricular failure (RVF) [1]. The adaptation of right ventricular function to increased afterload depends on the increased contractility by cardiomyocyte hypertrophy to match the increase in arterial elasticity. However, hypertrophic right ventricle will develop into RV–arterial uncoupling, which eventually leads to right ventricular dilation and RVF [2]. Primary pulmonary vascular lesions are believed to be the root cause of right heart failure due to PAH. A large number of studies have been devoted to elucidating the pathogenesis of progressive pulmonary vascular thickening in patients with PAH [3–5]. However, clinical evidence suggests that treating only the pulmonary vascular phenotype could not significantly improve the long-term survival of PAH patients [6]. Even with the improvements in pulmonary hemodynamic status, poor right ventricular function persists in PAH patients and deteriorates the prognosis [7]. Therefore, it is the focus of current research how to alleviate the adverse myocardial remodeling of right heart in PAH patients to eventually improve the prognosis of the disease.

Tumor cells and myocardial cells under pathological conditions both exhibit high expression of M-type pyruvate kinase 2 (PKM2) [8, 9], which catalyzes a rate-limiting step of glycolysis to produce pyruvate and adenosine triphosphate (ATP) from phosphoenolpyruvate and adenosine diphosphate (ADP). PKM2 oscillates among tetrameric, dimeric and monomeric forms [10]. The tetrameric form of PKM2 exerts the enzyme activity of glycolysis [11, 12]. However, in tumor cells, elevated oxidative stress could destabilize PKM2 tetramer through redox modifications on its cysteine residues [8, 10, 13]. Reduced catalytic activity of PKM2 thus diverts glucose metabolism flux towards the pentose phosphate pathway to generate adequate reducing power against reactive oxygen species (ROS), thus facilitating tumor cell proliferation. Oxidative stress and energetic metabolism reprogramming are well documented during the progression of heart failure [14]. Cardiomyocyte apoptosis induced by ROS is the common mechanism of decompensation of left and right heart failure [15]. Interestingly, elevated expression of PKM2 and enhanced tetramerization alleviate heart failure and improve myocardial regeneration [16–19], but detailed molecular mechanisms are incompletely understood.

In the present study, we further investigated the underlying molecular mechanisms through which PKM2 regulates cardiac function during right heart failure and explored whether leveraging PKM2 tetramerization

might serve as an effective approach to improve cardiac function.

Methods and materials

Animal model

Sprague–Dawley (SD) rats (weighing 220–250 g) from the Department of Laboratory Animals of Central South University (Changsha, China) were employed. All animal experiments were carried out in accordance with the recommendations of national and international animal care and ethical guidelines and were approved by the Ethics Committee for Animal Research of Xiangya Hospital of Central South University (permit code: 2103590). Monocrotaline (MCT, 55 mg/kg; C2401, powder, Sigma-Aldrich) was dissolved in saline containing 20% ethanol, and intraperitoneally injected into SD rats to establish PAH as described previously [20]. Animal experiments were performed in three batches with 5–6 rats per group (either the control group with solvent and the RVF group, or the RVF group with solvent and the RVF+TEPP-46 group). All rats were housed at 25 ± 2 °C with a 12-h light–dark cycle and free access to food and water. Transthoracic echocardiography was performed every 7 days to measure the maximum velocity of tricuspid regurgitation before day 21, and every 2 days after day 21. A maximum tricuspid regurgitation velocity greater than or equal to 2.5 m/s was the criterion for successful establishment of the PAH model. Right ventricular function was determined by measuring the fractional area change (FAC), the ratio between the difference in end-diastolic and end-systolic area and the end-diastolic area of the right ventricle. Right ventricular tissues were harvested at day 28. At the end of transthoracic echocardiography, the rats were euthanized with anesthetics, the heart tissues were collected. The rest parts of the body were bio-safely disposed by the Department of Laboratory Animals of Central South University.

Analysis of right ventricular systolic pressure and cardiac function

We used transthoracic echocardiography to collect and analyze right ventricular systolic pressure and function data in rats as previously described [20]. All rats were anaesthetized by inhalation of 6% to 8% (v/v) sevoflurane, and anaesthesia was maintained with 2% (v/v) sevoflurane. All rats were placed on a heating pad to maintain a body temperature of 37 °C. Echocardiography was performed with the Vivid E7 system (General Electric Vingmed). Right ventricular systolic pressure (RVSP) was equal to cross-valve pressure plus an estimated right atrial pressure (RAP) of 10 mmHg. Cross-valve pressure was estimated by calculating the maximum velocity of the tricuspid regurgitant

(TRmax) jet using the modified Bernoulli equation. Right ventricular function was determined by measuring the fractional area change (FAC), the ratio between the value of end-diastolic right ventricular area (RVA_d) minus end-systolic right ventricular area (RVA_s) and end-diastolic area. The rats in control group had no tricuspid regurgitation, we directly assessed the right ventricular end-systolic pressure using right ventricular catheterization technique. The monitoring data was collected and analyzed using LabChart 8 (ADInstruments).

Quantitative mass spectrometry

According to the data measured by echocardiography, right ventricular tissue (male, 6–8 weeks old, $n=3$) were collected at day 28 from euthanized rats and shipped to Jingjie PTM-Biolab for 4D label-free quantitative proteomic analysis. Samples were subjected to standard protein extraction and trypsin digestion [21]. The tryptic peptides were desalted by C18 SPE column and were subsequently dissolved in solvent A (0.1% formic acid, 2% acetonitrile), directly loaded onto a home-made reversed-phase analytical column (25-cm length, 75/100 μm i.d.). Peptides were separated with a gradient from 6 to 24% solvent B (0.1% formic acid in acetonitrile) over 70 min, 24% to 35% in 14 min and climbing to 80% in 3 min then holding at 80% for the last 3 min, all at a constant flow rate of 450 nL/min on a nanoElute UHPLC system (Bruker Daltonics). The peptides were subjected to capillary source followed by the timsTOF Pro (Bruker Daltonics) mass spectrometry. Based on the Raw file obtained from mass spectrometry detection, a database of sample-specific proteins based on the origin was constructed for database search. Subsequently, quality control and quantitative analysis at the peptide and protein levels were performed on the matched results. Fold change (FC) and *t*-test were performed on the quantitative results. The false discovery rate (FDR) adjusted *p* value was calculated based on the Benjamini and Hochberg (BH) method [22]. Proteins with fold change (FC) above 1.5 or below 1/1.5 having more than one unique peptide were regarded to be differentially expressed (FDR-adjusted *p* value < 0.05).

TEPP-46 treatment

The PAH rats were randomly divided into two groups on the 21st day after MCT injection. The experimental group was given TEPP-46 (30 mg/kg; MedChem Express, HY-18657) gavage treatment every day, and the control group was given corresponding solvent gavage operation. Cardiac function data were obtained every 2 days, and right ventricular tissues were harvested on day 28.

Isolation, culture, and treatment of primary cardiac myocytes

Neonatal rat ventricular myocytes (NRVMs) were isolated from 1-day-old SD rats by using a neonatal heart dissociation kit (Miltenyi Biotec, 130-098-373) following the manufacturer's instructions and cultured in dulbecco's modified eagle medium (DMEM) (Gibco, 11965092) containing 10% fetal bovine serum (FBS) (Hyclone, SV30087.03), and 1% penicillin & streptomycin (AbioWell, AWH0529a). The cells were grown at 37 °C in a humidified atmosphere with 5% CO₂, and the medium was changed every two days. primary cardiac myocytes were exposed to arginine vasopressin (AVP, 1 μM , HY-P0049; MedChem Express) for up to 48 h to induce hypertrophy and TEPP-46 (100 μM) for 24 h to promote PKM2 tetramerization.

Western blotting analysis

Total protein was extracted from right ventricular tissues or myocytes with RIPA buffer (NCM, WB2100) containing 1 mM PMSF (Byotime, ST507), and protein concentration was determined by BCA protein assay kit (NCM, WB6501). Total proteins were separated on BeyoGel Plus PAGE Tris-Gly system (Byotime, 0469S) and transferred to a polyvinylidene fluoride (PVDF) membrane (Millipore, ISEQ00010). The membrane was blocked with 5% skim milk in PBS with 0.1% Tween 20 (PBST) at room temperature for 1 h and incubated with primary antibodies (Additional file 3: Table S1) at 4 °C overnight. The membrane was then incubated with peroxidase affiniPure goat anti-rabbit IgG (H+L) (1:10000, Jackson, 111-035-144) at room temperature for 1 h. Finally, enhanced chemiluminescence (ECL) reagent (Advansta, K-12045-D50) was used to detect the bands. All images of uncropped gels from figures could be reviewed in Additional file 6.

Crosslinking to determine PKM2 tetramer

As described in previous studies [23, 24], an equal amount of fresh heart right ventricular tissue or primary myocytes was used for crosslinking. Myocardial tissue was cut into 1 mm³ pieces with surgical scissors, then it was crosslinked with 2.5 mM DSS in PBS for 30 min at room temperature, with constant rotation. For primary myocytes, we used 500 μM DSS in PBS to crosslink. Samples were separated by BeyoGel Plus PAGE 4–20% Tris-Gly Gel (Beyotime, P0469S).

Quantitative real-time PCR

The total RNA of ventricular tissue was isolated using the Total RNA Kit II (R6934-01, Omega Bio-tek) according to the manufacturer's instructions. An RT Reagent Kit

with gDNA Eraser (RR047A, Takara) was used for cDNA synthesis. Real-time PCR was performed using All-in-One™ qPCR Mix (QP001, GeneCopoeia) according to the manufacturer's protocol. Primer sequences are listed in Additional file 4: Table S2.

Histology and immunochemistry

Paraffin-embedded sections were subjected to hematoxylin and eosin (HE) or Masson's trichrome staining. Images were acquired using a Nikon Eclipse E100 and a NIKON DS-U3 automated slide scanner.

TUNEL staining

The heart samples were separated and fixed in 10% phosphate-buffered formalin for 24 h, subsequently embedded in paraffin, and sliced (4–5 μm). Terminal deoxynucleotidyl transferase-mediated dextoxyuridine triphosphate nick-end labeling (TUNEL) staining was performed using the TUNEL BrightGreen Apoptosis Detection Kit (A112-01, Roche Life Science) following manufacturer's instructions. Apoptotic nuclei were labeled with green fluorescein staining and total cardiomyocyte nuclei were marked with 4',6'-diamidino-2-phenylindole (DAPI) (SouthernBiotech, 0100-20). The slices of heart tissues were viewed by confocal microscopy (Eclipse C1, NIKON). The rate of apoptosis was displayed as the percentage of TUNEL positive nuclei in DAPI-stained nuclei.

Flow cytometry analysis

Cells were digested with trypsin without EDTA and washed twice with PBS. Apoptosis of myocytes was detected by PE Annexin V Apoptosis Detection Kit I (BD Biosciences, 559,763) following the manufacturer's instructions. Flow cytometry analysis was performed on a DxP Athena™ instrument (Cytekbio), and the data were analysed using FlowJo software. Annexin V with PE staining was monitored at emission wavelength of 578 nm and an excitation wavelength of 488 nm. 7-Amino-Actinomycin (7-AAD) was monitored at emission wavelength of 647 nm and an excitation wavelength of 488 nm. Cells negative for Annexin V and 7-AAD staining were deemed to be viable. Cells in early apoptosis displayed positive for Annexin V while maintaining negative for 7-AAD staining. Conversely, cells in late apoptosis exhibit positive staining for both Annexin V and 7-AAD.

Transmission electron microscopy (TEM) and evaluation of damaged mitochondria

Fresh heart right ventricle samples were fixed in 2.5% glutaraldehyde (pH 7.4) for 2 h. Samples were then washed three times with 0.1 M phosphate buffer (pH 7.2)

and fixed in 1% osmic acid at 4 °C for 2 h. Subsequently, the samples were gradient dehydrated in a graded series of ethanol, embedded in Epon-Araldite resin for penetration and placed in a mold for polymerization. After the semi thin section was used for positioning, the ultrathin section was made and collected for microstructure analysis, followed by the counterstaining of 3% uranyl acetate and 2.7% lead citrate. Data were acquired with a Hitach HT7800 transmission electron microscope.

Healthy mitochondria exhibit intact and well-defined membranes, along with abundant and regular cristae. Swollen mitochondria, on the other hand, display distorted membranes and disrupted or enlarged cristae. Vacuolar mitochondria are characterized by the separation of inner and outer mitochondrial membranes, accompanied by the absence of cristae. To quantify damaged mitochondria, the ratio of vacuolar and swollen mitochondria to the total number of mitochondria in the image was computed. Ruptured mitochondria exhibit a discontinuity in the outer mitochondrial membrane. To quantify ruptured mitochondria, the ratio of ruptured mitochondria to the total number of mitochondria in the image was calculated.

Advanced oxidation protein product (AOPP) measurement

AOPP test was used to assess oxidative stress within the right ventricular tissues according to the manufacturer's instructions. Right ventricular myocardial tissue samples (20–30 mg) were harvest for homogenization. Then, we collected the supernatant for AOPP measurements using the AOPP assay kit (Abcam, ab242295). Results were normalized by protein concentration.

ROS measurement in primary cardiac myocytes

Cells were seeded in 35 mm glass-bottomed culture dish with a density of 5×10^4 /ml. Cells were incubated with 5 μM MitoSOX Red (Invitrogen, M36008) for 10 min at 37 °C. The cells were washed twice with PBS, and the fluorescence imaging of live primary cardiomyocyte was conducted at 510/580 nm on Axio Observer 7 microscope (Zeiss). The mean fluorescence intensity of cells was quantified using Fiji software.

Immunofluorescence

Cells were stained with 100 nM MitoTracker Red (Invitrogen, M7512) for 30 min, fixed for 10 min with 4% paraformaldehyde and permeabilized with 0.1% Triton X-100 for 10 min. For OPA1 staining, cells were incubated with specific primary antibody (CST, 67589S) overnight in 1% BSA at 4 °C, followed by secondary antibody (Invitrogen, A11034) at room temperature for 1 h. DNA was stained with DAPI. Images were acquired using Apotome

microscope (Zeiss). As previously described, the means of area, perimeter, aspect ratio and form factor of mitochondria were quantified using Mitochondria Analyzer in Fiji software according to the published protocol [25–27].

Statistical Analysis

All replicate data are expressed as the means \pm standard error of the mean (SEM). The distribution of the data was assessed with the Shapiro–Wilk normality test. The significance of difference between two independent experimental groups was assessed using unpaired Welch's t-test, and the significance of difference among more than two groups was assessed using one-way ANOVA. The data between two groups with repeated measurements were compared using two-way ANOVA. The value of statistical significance was set at $p < 0.05$. *, ** and *** represents $p < 0.05$, < 0.01 , and < 0.001 , respectively. Statistical analyses were performed using GraphPad Prism 9 software.

Results

Oxidative stress and mitochondrial disorganization are associated with increased apoptosis in the right ventricular tissue of RVF rats

To establish the animal model of RVF, we induced PAH in rats by intraperitoneal injection of MCT as in previous studies [28, 29] (Fig. 1A). The elevation of pulmonary artery pressure was confirmed through transthoracic ultrasound examination and right heart catheterization (Additional file 1: Fig. S1A, B). RVF rats exhibited tricuspid regurgitation on ultrasound imaging starting from day 21 after MCT injection (Additional file 1: Fig. S1C), accompanied by a rapid deterioration in cardiac function

(Fig. 1B–D). HE and Masson staining showed severe loss of cardiomyocytes and accumulation of fibrous components in the right heart tissue of RVF rats comparing to the control group (Fig. 1E, F). Apoptosis was significantly activated in the right ventricular tissue of RVF rats (Fig. 1G, H). Correspondingly, the expression of proapoptotic proteins (BAX, caspase-3 and caspase-7) was increased, while the level of anti-apoptotic protein Bcl-2 was downregulated (Fig. 1I, J). Meanwhile, the oxidative stress level was significantly upregulated in the right ventricular tissue of RVF rats, accompanied by the disorganized mitochondria with reduced density, significantly increased swelling, vacuolization and rupture of outer membrane (Fig. 1K–O).

PKM2 is upregulated during right ventricular failure and negatively correlated with the cardiac function

To explore the molecular mechanisms regulating heart failure progression, the right ventricular tissues of RVF rats and control group were subjected to 4D label-free quantitative liquid chromatography-mass spectrometry analysis. Principal component analysis (PCA) showed distinct proteomic profile between RVF rats and control (Additional file 1: Figure S1D). Proteins with FC above 1.5 or below its reciprocal having more than one unique peptide were regarded to be differentially expressed (FDR-adjusted p value < 0.05). Among the 2253 identified proteins, 635 were upregulated and 489 were downregulated comparing RVF rats and control group (Fig. 2A, Additional file 5: Table S3). As expected, proteins known to be involved in heart failure were enriched. The proteins regulating calcium ion cycle and contraction unit (ATP2A2, RYR2, TNNC1 and TTN) were significantly downregulated, while the proteins involved in

(See figure on next page.)

Fig. 1 Oxidative stress and mitochondrial disorganization are associated with increased apoptosis in the right ventricular tissue of RVF rats. **A** Schematic diagram of the pulmonary hypertension-induced RVF rat model established by intraperitoneal injection of MCT. Transthoracic echocardiography was carried out as indicated. The right ventricular tissues were harvested on day 28 for analysis. **B–C** Right ventricular function was determined by measuring the fractional area change (FAC). Results are expressed as mean \pm SEM, $n = 6$ rats per group. **D** Pulmonary artery pressure was measured using right heart catheterization. Results are expressed as mean \pm SEM, $n = 4–5$ rats per group. **E–F** Paraffin-embedded sections of heart tissue were subjected to HE or Masson staining. The boxed area was further enlarged. Scale bar (left panel) = 100 μ m; scale bar (right panel) = 2000 μ m. **G** Apoptosis was measured by TUNEL staining (green) at paraffin-embedded sections. Nuclei were stained with DAPI in blue. Scale bar (left panel) = 100 μ m; scale bar (right panel) = 50 μ m. **H** The quantification of G. Data was collected from ten random fields from the right ventricular tissue section of two rats per group. **I–J** Lysates from right ventricle of control and RVF rats were analyzed by western blotting with indicated antibodies. Relative protein level was quantified and expressed as mean \pm SEM, $n = 3$ rats per group. **K** Relative ROS level in right ventricular tissue was measured by AOPP test. Results are expressed as mean \pm SEM, $n = 6–7$ rats per group. **L** TEM of right ventricle from control and RVF rats (scale bar = 1 μ m). Damaged mitochondria were marked with black arrow head, ruptured mitochondria were marked with red arrow head. **M** The total count of mitochondria in field were calculated according to representative transmission electron micrographs of right ventricular tissues of rat in control and RVF group. Results are expressed as mean \pm SEM, $n = 10$ micrographs per group. **N** The ratio of damaged mitochondria to total mitochondria (black arrows) in field were calculated according to representative transmission electron micrographs of right ventricular tissues of rat in control and RVF group. Results are expressed as mean \pm SEM, $n = 10$ micrographs per group. **O** The ratio of ruptured mitochondria to total mitochondria (red arrows) in field were calculated according to representative transmission electron micrographs of right ventricular tissues of rat in control and RVF group. Results are expressed as mean \pm SEM, $n = 10$ micrographs per group

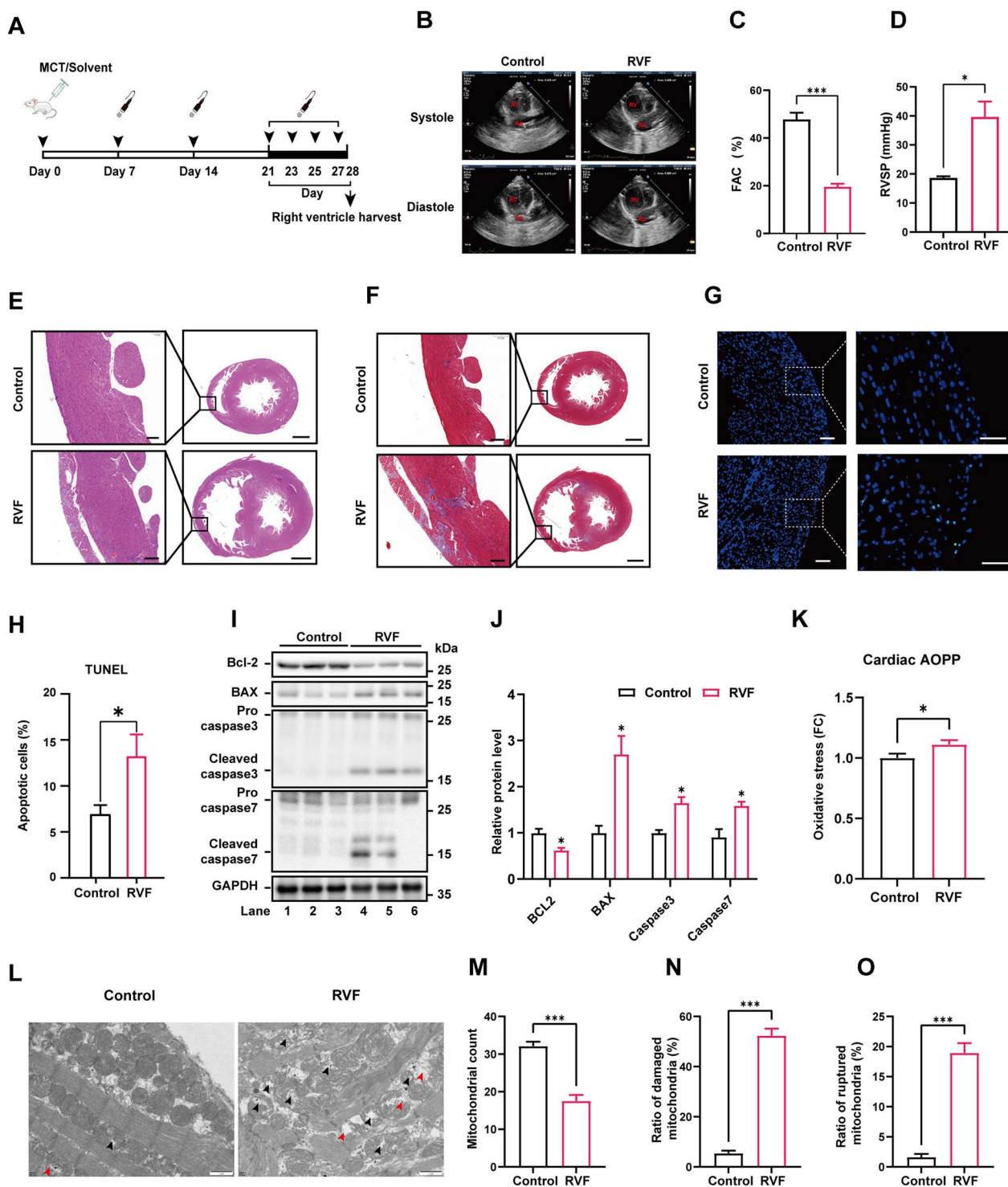


Fig. 1 (See legend on previous page.)

cardiomyocyte hypertrophy, fibrosis and transcription reprogramming (MYH7, FN1, LGALS3 and PTBP1) were significantly upregulated (Fig. 2B) [30–35]. Moreover, the expression level of genes involved in myocardial

contractile function was analyzed by RT-qPCR. The expression of *Atp2a2*, *Ryr2*, *Myh6*, *Tnnt3* and *Tnni3* was significantly downregulated in RVF rats, indicating the myocardial contractility was severely impaired

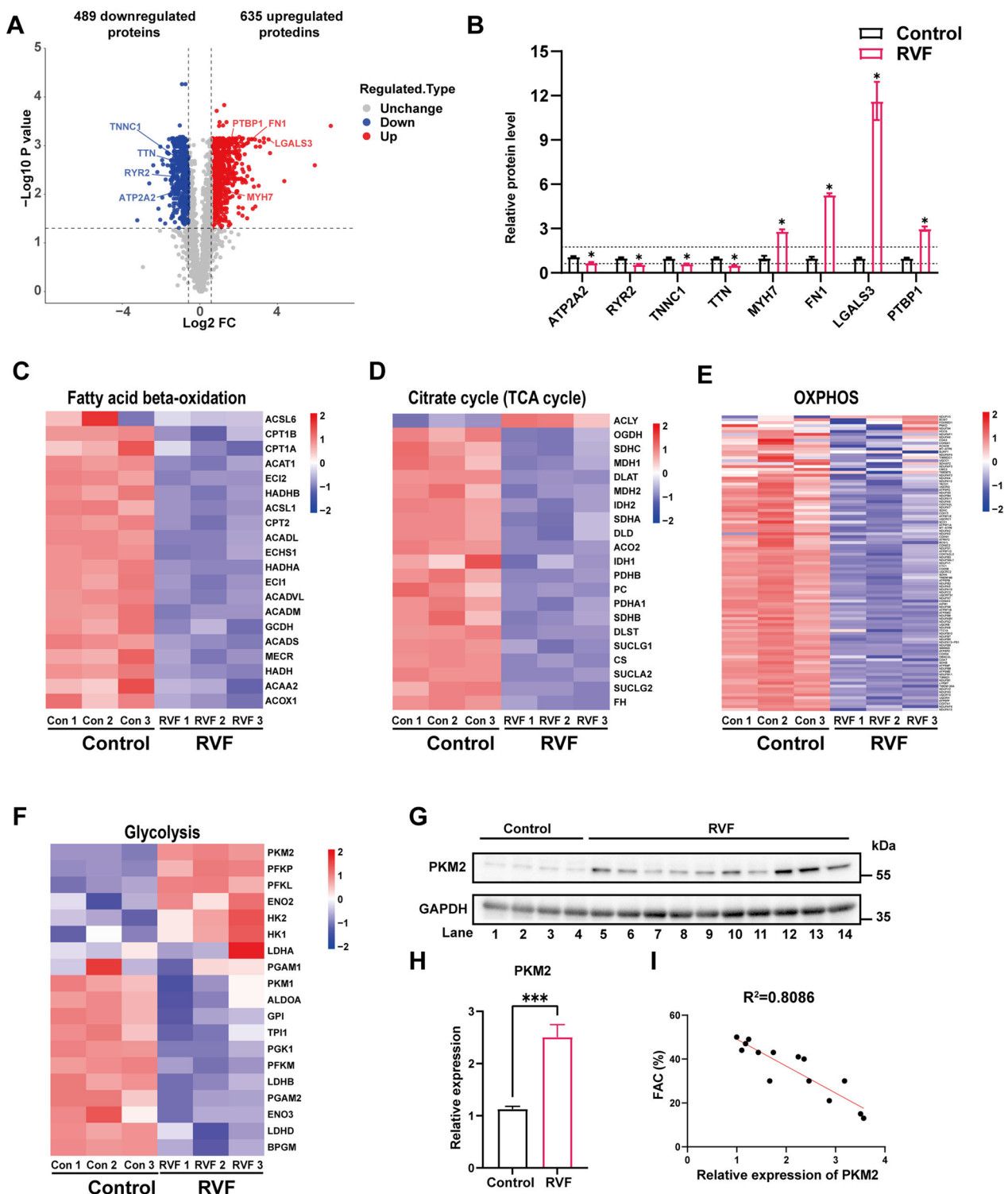


Fig. 2 Quantitative proteomics reveals that PKM2 is upregulated during right ventricular failure and negatively correlated with the cardiac function. **A** The volcano plot of proteins quantified by mass spectrometry from right ventricular tissue of control and RVF rats. **B** Relative abundance of proteins known to be involved in heart failure from mass spectrometry. The dash lines represent the upregulation and downregulation thresholds. **C–F** Heatmaps of differentially expressed proteins related to fatty acid beta-oxidation, TCA cycle, OXPHOS and glycolysis from mass spectrometry. **G–H** Lysates from right ventricle of control and RVF rats were analyzed by western blotting with indicated antibodies. Relative protein level was quantified and expressed as mean \pm SEM, n = 4 rats in control group, n = 10 in RVF group. **I** The relative protein level of PKM2 was negatively correlated with the right ventricular function

(Additional file 1: Fig. S1E). Importantly, most proteins participated in fatty acid oxidation, tricarboxylic acid cycle (TCA) cycle and oxidative phosphorylation (OXPHOS) were significantly downregulated (Fig. 2C–E), indicating a reprogramming of energy metabolism away from mitochondrial respiration in the right ventricular tissue of RVF rats [14]. Indeed, key enzymes of glycolysis including PKM2 (but not PKM1) were significantly upregulated (Fig. 2F–H, Additional file 1: S1F, G). The PKM2 protein level was negatively correlated with the right ventricular function (Fig. 2I), indicating an important role of PKM2 during heart failure progression.

Promoting PKM2 tetramerization alleviates oxidative stress and apoptosis during cardiomyocyte hypertrophy

Cardiomyocyte hypertrophy is a key phenotype in the progression of heart failure. To further study the molecular mechanism underlying the function of PKM2, we stimulated NRVMs with AVP to induce hypertrophy as in previous studies [36, 37]. Application of AVP effectively induced cardiomyocyte hypertrophy (Fig. 3A, B), oxidative stress (Fig. 3C, D) and apoptosis (Fig. 3E–G). Unlike in the RVF rats, cardiomyocyte hypertrophy induced by AVP did not upregulate the steady level of PKM2, while MYH7 expression was increased (Fig. 3H–J). Interestingly, PKM2 tetramerization was significantly downregulated in cardiomyocyte hypertrophy as well as in the right ventricular tissue of RVF rats (Fig. 3K–N). The destabilization of PKM2 tetramer promotes tumor growth under oxidative stress [8, 10, 13]. To analyze the function of PKM2 tetramerization in cardiomyocyte hypertrophy, rat primary cardiomyocytes were further treated with TEPP-46 following AVP stimulation to promote PKM2 tetramerization (Fig. 3O, P) [24, 38]. Surprisingly, unlike in tumor cells, promoting PKM2 tetramerization alleviated the oxidative stress and accompanied apoptosis during cardiomyocyte hypertrophy (Fig. 3Q–U).

Facilitating PKM2 tetramerization promoted mitochondrial network formation by regulating mitochondrial fission and fusion machineries

Oxidative stress is intimately connected to mitochondrial morphology. We thus analyzed AVP treated cardiomyocytes via immunofluorescence and stained for mitochondrial specific markers (mitochondrial protein OPA1 and MitoTracker Red). Mitochondrial network was found to be more fragmented in hypertrophic cardiomyocytes (Additional file 2: Fig. S2A). Mean mitochondrial area and mean mitochondrial perimeter in hypertrophic cardiomyocytes were significantly lower than those in control cells (Additional file 2: Fig. S2B, C), and the decrease in mean form factor and mean aspect ratio suggested that the mitochondria in hypertrophic cardiomyocytes were more spherical in shape, indicating increased mitochondrial fission in cardiomyocyte hypertrophy (Additional file 2: Fig. S2D, E). Accordingly, the expression of Drp1 and cleaved OPA1 was elevated in AVP treated cardiomyocytes, which was consistent with the increased mitochondrial fission in hypertrophic cardiomyocytes (Additional file 2: Fig. S2F–I). To analyze how PKM2 tetramerization regulates mitochondrial dynamics in hypertrophic cardiomyocytes, PKM2 tetramerization was promoted by TEPP-46 following AVP stimulation. Importantly, enhanced PKM2 tetramerization suppressed mitochondrial fission in hypertrophic cardiomyocytes (Fig. 4A–E). Meanwhile, western blotting analysis demonstrated the increased expression of Drp1 and the elevated cleavage of OPA1 were both rescued by TEPP-46 treatment (Fig. 4F–I). Taken together, facilitating PKM2 tetramerization promoted mitochondrial network formation by regulating mitochondrial fission and fusion machineries.

(See figure on next page.)

Fig. 3 Promoting PKM2 tetramerization alleviates oxidative stress and apoptosis during cardiomyocyte hypertrophy. **A** Rat primary cardiomyocytes were treated with 1 μ M AVP for 48 h to induce hypertrophy. Scale bar = 200 μ m. **B** The diameter of cardiomyocytes in A was measured. Results are expressed as mean \pm SEM, n = 20 cells per group. **C–D** The ROS level was analyzed by MitoSOX Red. Scale bar = 20 μ m. Quantitative results are expressed as mean \pm SEM, n = 20 cells per group. **E–G** The apoptosis of cardiomyocytes was analyzed by flow cytometry. Quantitative results are expressed as mean \pm SEM, n = 3. **H–J** Lysates from primary cardiomyocytes were analyzed by western blotting with indicated antibodies. Relative protein level was quantified and expressed as mean \pm SEM, n = 3. **K–L** As in previous studies, PKM2 tetramerization was analyzed by DSS crosslinking of primary cardiomyocytes. The ratio of tetramer to monomer was quantified and expressed as mean \pm SEM, n = 3. **M–N** PKM2 tetramerization in the right ventricular tissue of control and RVF rats was analyzed by DSS crosslinking. The ratio of tetramer to monomer was quantified and expressed as mean \pm SEM, n = 4 rats per group. **O–P** Rat primary cardiomyocytes were treated with 1 μ M AVP for 48 h and 100 μ M TEPP-46 for 24 h as indicated. PKM2 tetramerization was analyzed by DSS crosslinking. **Q–R** The ROS level was analyzed by MitoSOX Red. Scale bar = 20 μ m. Quantitative results are expressed as mean \pm SEM, n = 20 cells per group. **S–U** The apoptosis of cardiomyocytes was analyzed by flow cytometry. Quantitative results are expressed as mean \pm SEM, n = 3

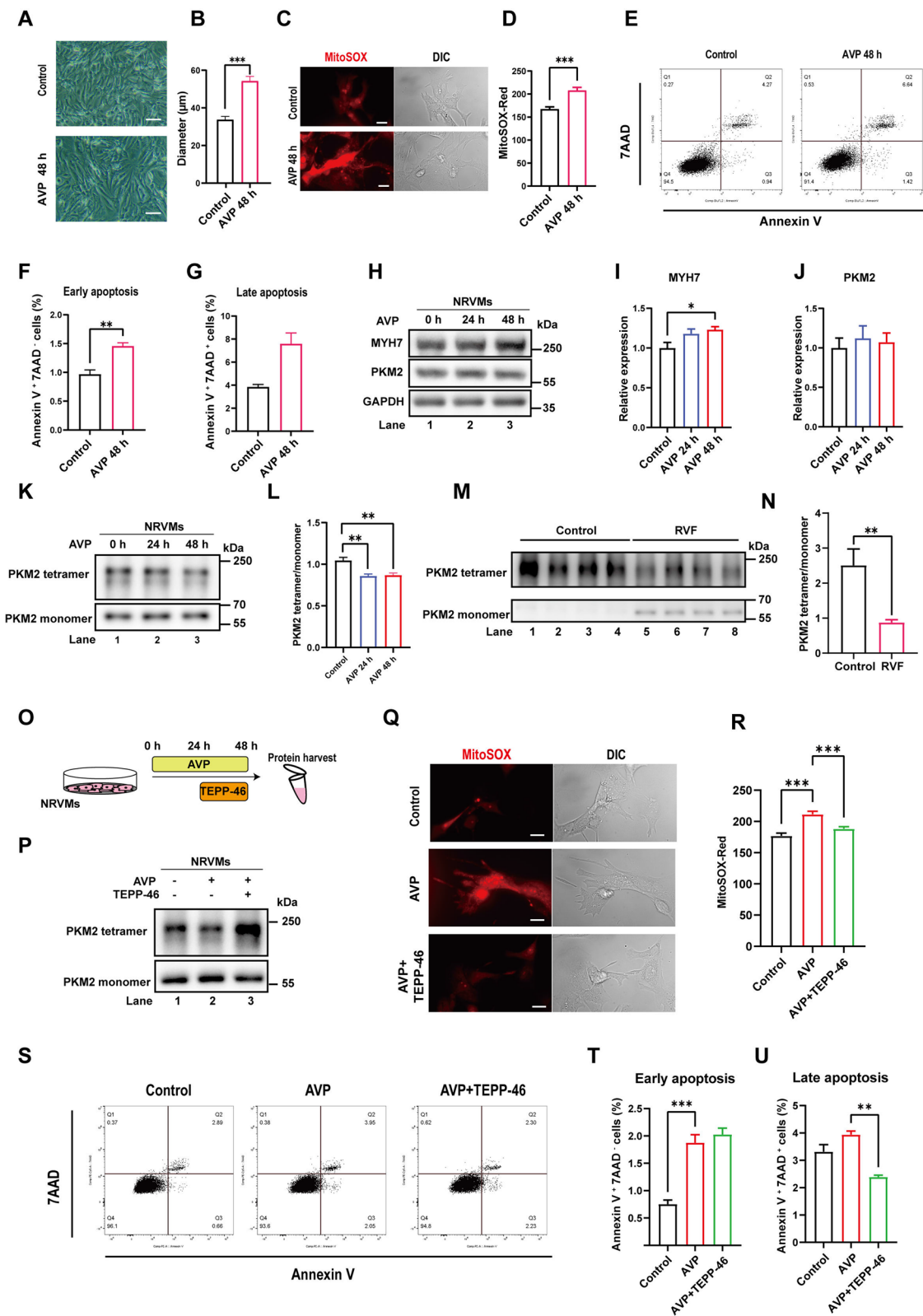


Fig. 3 (See legend on previous page.)

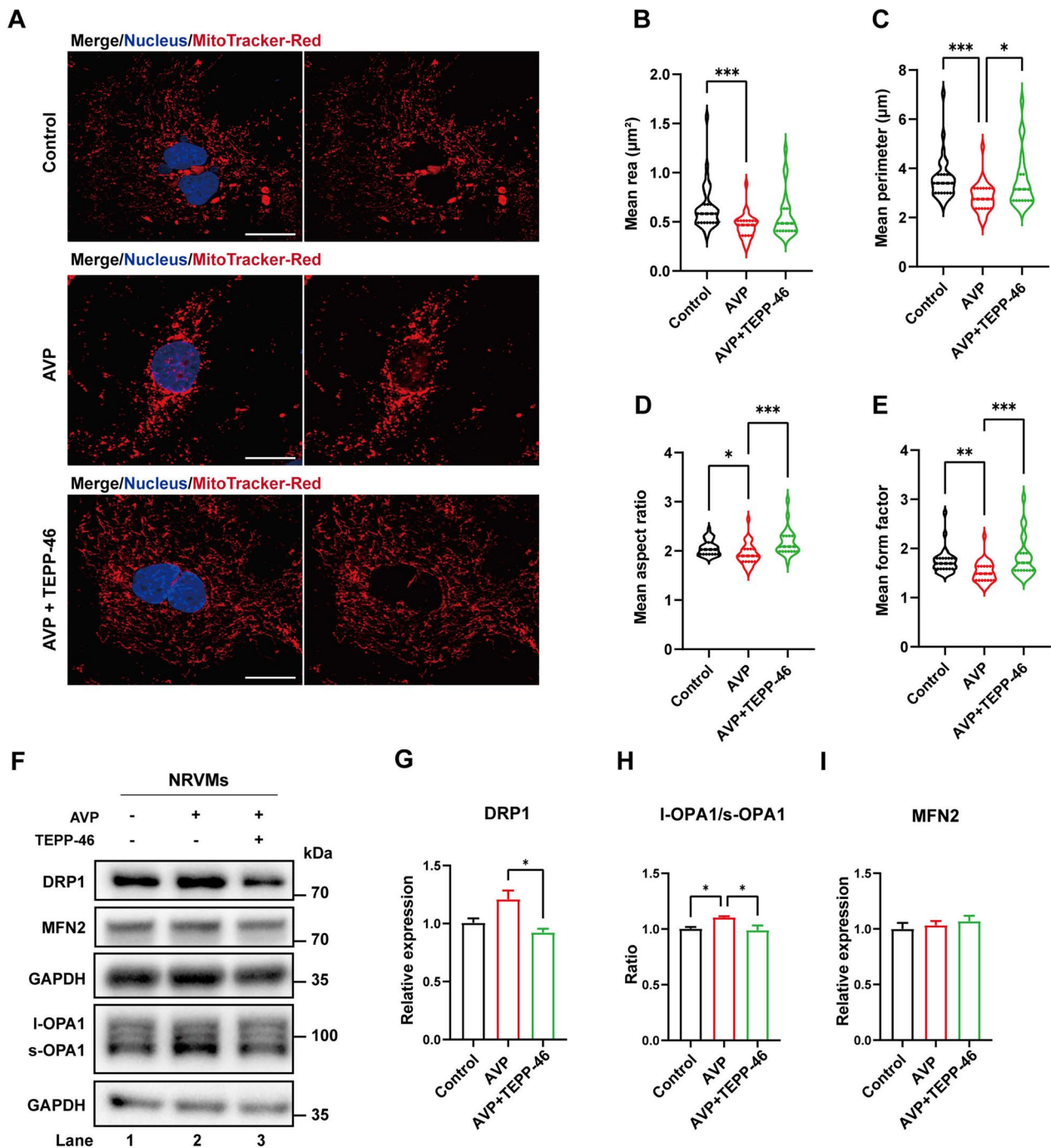


Fig. 4 Facilitating PKM2 tetramerization promoted mitochondrial network formation. **A** Rat primary cardiomyocytes were treated with AVP and TEPP-46 as indicated and stained by MitoTracker-Red to visualize mitochondrial morphology. Scale bar = 20 μm . **B-E** The means of area, perimeter, aspect ratio and form factor of mitochondria were quantified. Results are expressed as mean \pm SEM, $n = 25$ cells per group. **F-I** Lysates from primary cardiomyocytes were analyzed by western blotting with indicated antibodies. Relative protein level was quantified and expressed as mean \pm SEM, $n = 3$

Enhancing PKM2 tetramer formation improves cardiac mitochondrial morphology, mitigates oxidative stress and alleviates heart failure

To investigate whether the deterioration of cardiac function in RVF rats could be alleviated by promoting PKM2 tetramerization, TEPP-46 was administered (30 mg/kg, once per day) by gavage from day 21 to day 27 after intraperitoneal injection of MCT, while the control RVF rats were given the corresponding solvent (Fig. 5A). The right ventricular function was measured every 2 days from day 21. Oral administration of TEPP-46 promoted PKM2 tetramerization in the right ventricular tissue of RVF rats (Fig. 5B, C), and significantly delayed the deterioration of cardiac function without affecting the pulmonary artery pressure (Fig. 5D, Additional file 1: S1H, I). The cardiomyocyte loss and the accumulation of fibrous components in the right ventricular tissue of RVF rats were alleviated via TEPP-46 administration (Fig. 5E, F). Accordingly, TUNEL staining revealed that the apoptosis of cardiomyocyte was decreased with TEPP-46 treatment (Fig. 5G, H), with lower level of oxidative stress in the right ventricular tissue (Fig. 5I). Meanwhile, the dysregulation of anti-apoptotic and proapoptotic proteins in the right ventricular tissue of RVF rats was partially rescued after TEPP-46 administration (Fig. 5J, K). Moreover, the morphological abnormality of mitochondria was largely rescued by promoting PKM2 tetramer formation (Fig. 5L–O). Taken together, enhancing the tetramerization of PKM2 improved mitochondrial morphology, mitigated the oxidative stress related cardiomyocyte apoptosis, and alleviated the deterioration of cardiac function during heart failure progression (Fig. 6).

Discussion

Right heart failure is primarily caused by pulmonary arterial hypertension and is the leading cause of mortality in affected patients [39]. The increased afterload, along with various endocrine hormones, promotes hypertrophy of myocardial cells. However, hypertrophied myocardial cells eventually progress towards apoptosis, leading to the decompensation of heart function [40–42]. Mitochondrial damage and excessive accumulation of ROS are known to promote myocardial cell apoptosis, which is a key event in the decompensation of heart function [15, 43, 44]. Therefore, proper regulation of mitochondrial quality control and oxidative stress in myocardial cells may be important aspects for preserving heart health and delaying the progression of heart failure. In recent years, numerous studies have reported that the upregulation of PKM2 in the pathological state of the heart plays crucial roles in the occurrence and progression of various types of heart failure [8, 17–19, 44–46]. However, the associated molecular mechanisms are not completely understood.

MCT serves as a classic animal model for pulmonary hypertension. The elevated RVSP induced by MCT in our study align with previous reported findings [28, 29]. Via quantitative proteomics, we observed that the expression of PKM2 was upregulated in the progression of RVF and was negatively correlated with the cardiac function. Interestingly, the tetramerization of PKM2 was significantly downregulated both in cardiomyocyte hypertrophy and in the right ventricular tissue of RVF rats. In tumor cells, the destabilization of PKM2 tetramer restricts its catalytic activity in glycolysis, diverts glucose carbon into the pentose phosphate pathway for NADPH

(See figure on next page.)

Fig. 5 Oral administration of TEPP-46 alleviates heart failure, improves cardiac mitochondrial morphology and mitigates oxidative stress. **A** Schematic diagram of the TEPP-46 treatment for RVF rats. Transthoracic echocardiography was carried out as indicated. The right ventricular tissues were harvested on day 28 for analysis. **B–C** PKM2 tetramerization in the right ventricular tissue of RVF and RVF + TEPP-46 rats were analyzed by DSS crosslinking. The ratio of tetramer to monomer was quantified and expressed as mean \pm SEM, $n = 5$ rats per group. **D** Right ventricular function of RVF rats treated with or without TEPP-46 was determined by measuring the FAC at indicated time. Significance was determined by two-way ANOVA followed by Sidak's multiple comparisons test, $n = 5$ rats per group. **E–F** Paraffin-embedded sections of heart tissue were subjected to HE or Masson staining. The boxed area was further enlarged. Scale bar (left panel) = 100 μm ; scale bar (right panel) = 2000 μm . **G** Apoptosis was measured by TUNEL staining (green) at paraffin-embedded sections. Nuclei were stained with DAPI in blue. Scale bar (left panel) = 100 μm ; scale bar (right panel) = 50 μm . **H** The quantification of F. Data was collected from ten random fields of the right ventricular tissue section of two rats per group. **I** Relative ROS level in right ventricular tissue was measured by AOPP test. Results are expressed as mean \pm SEM, $n = 6$ rats per group. **J–K** Lysates from right ventricle of RVF rats treated with or without TEPP-46 were analyzed by western blotting with indicated antibodies. Relative protein level was quantified and expressed as mean \pm SEM, $n = 3$ rats per group. **L** TEM of right ventricle in RVF and RVF + TEPP-46 rats (Scale bar = 1 μm). Damaged mitochondria were marked with black arrow head, ruptured mitochondria were marked with red arrow head. **M** The total count of mitochondria in field were calculated according to representative transmission electron micrographs of right ventricular tissues of rat in RVF and RVF + TEPP-46 group. Results are expressed as mean \pm SEM, $n = 10$ micrographs per group. **N** The ratio of damaged mitochondria to total mitochondria (black arrows) in field were calculated according to representative transmission electron micrographs of right ventricular tissues of rat in RVF and RVF + TEPP-46 group. Results are expressed as mean \pm SEM, $n = 10$ micrographs per group. **O** The ratio of ruptured mitochondria to total mitochondria (red arrows) in field were calculated according to representative transmission electron micrographs of right ventricular tissues of rat in RVF and RVF + TEPP-46 group. Results are expressed as mean \pm SEM, $n = 10$ micrographs per group

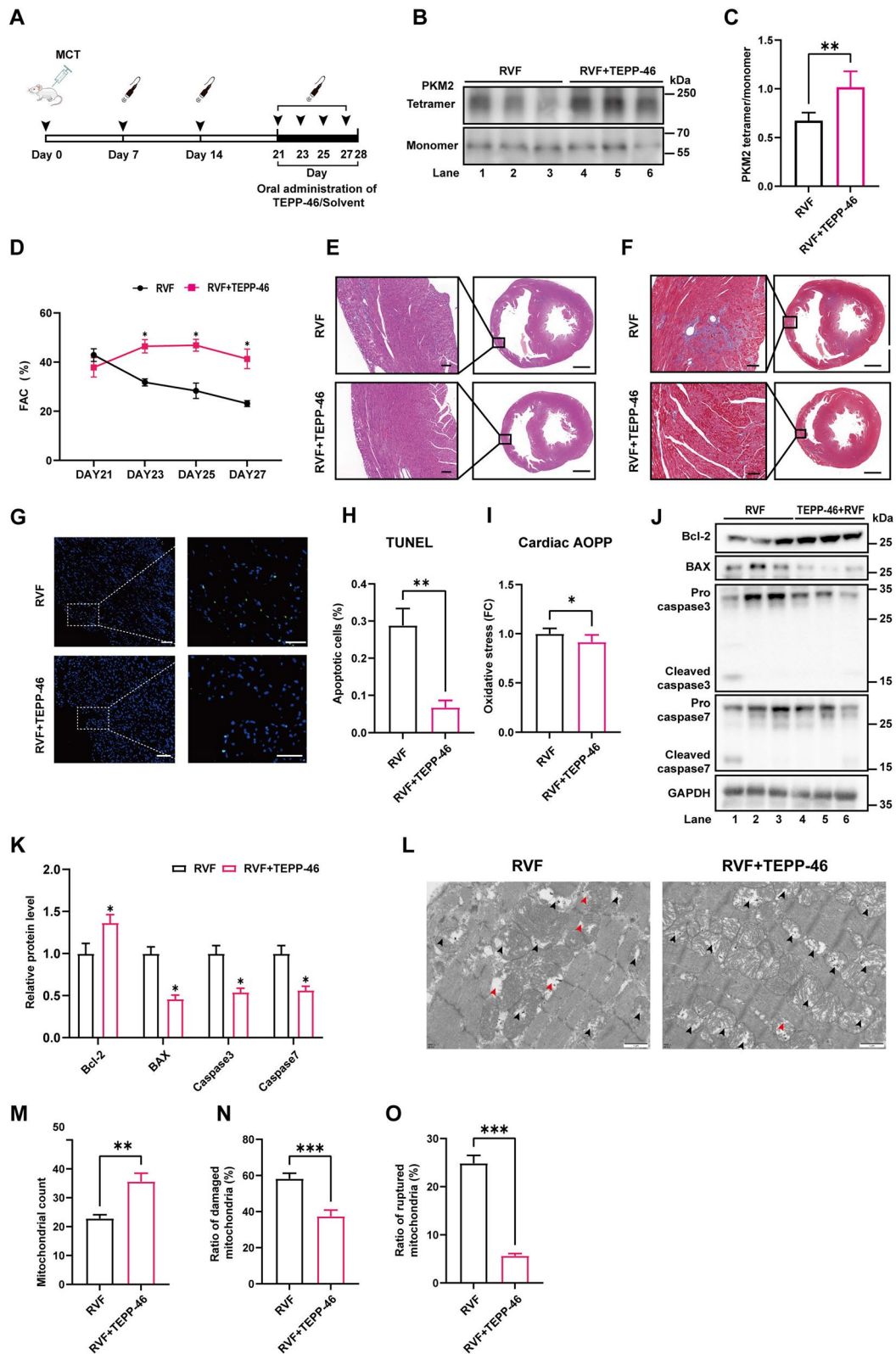


Fig. 5 (See legend on previous page.)

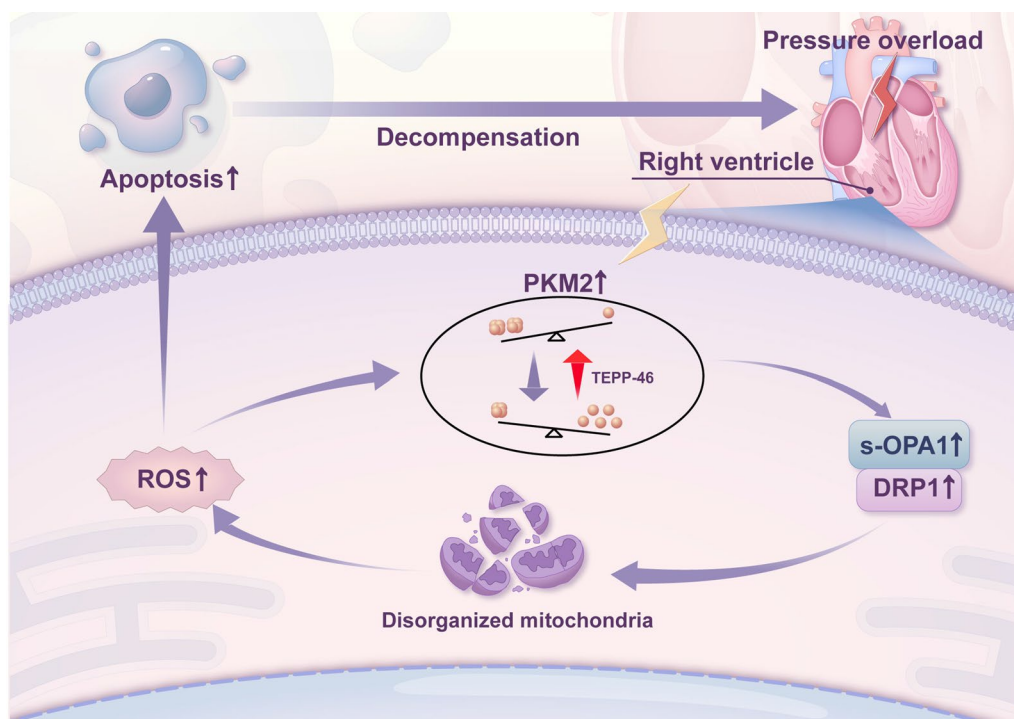


Fig. 6 Schematic model of promoting PKM2 tetramerization alleviates the decompensation of cardiac function by regulating oxidative stress and mitochondrial dynamics. Pressure overloading induces cardiomyocyte hypertrophy with upregulated PKM2 level, and the tetrameric proportion of PKM2 is reduced by intracellular oxidative stress. An imbalanced ratio of PKM2 tetramer/monomer upregulates Drp1 level and increases OPA1 cleavage, and ultimately leads to mitochondria disorganization and elevated ROS level. This vicious cycle eventually accelerates the apoptosis of cardiomyocytes and promotes cardiac function into the decompensated phase. The application of TEPP-46 can improve mitochondrial network formation, mitigates oxidative stress and alleviates the decompensation of cardiac function via enhancing PKM2 tetramer formation

production, thus is important for the adaptive response of tumor cells against oxidative stress to promote tumor cell proliferation and tumor growth [8, 48]. However, the adaptation of oxidative stress in cardiomyocyte seems to be differently regulated. Unlike in tumor cells, we observed that facilitating PKM2 tetramerization in cardiomyocytes alleviated oxidative stress. The exact molecular mechanisms behind this phenomenon are not clear, but the function of mitochondrial dynamic control is worthy of further studies, since stabilization of PKM2 tetramer improved mitochondrial network formation and mitigated apoptosis and heart failure.

Proper mitochondrial dynamic control is crucial for healthy cardiac function [48]. The abnormal regulation of mitochondrial fusion/fission machineries is intimately associated with mitochondrial dysfunction during heart failure [49–53]. In our study, the increased mitochondrial fragmentation in hypertrophic cardiomyocytes was accompanied by the elevated level of DRP1 expression and OPA1 cleavage, which were effectively rescued by promoting PKM2 tetramerization with TEPP-46. Although we did not observe any alteration on MFN2

by TEPP-46, it does not rule out the impact of PKM2 tetramerization on the fusion machineries of mitochondrial outer membrane. Indeed, in tumor cells, it has been reported that PKM2 could translocate to mitochondria and interact with MFN2 to promote mitochondrial fusion and energy production [54]. In addition, PKM2 has also been reported to stabilize Bcl-2, thus inhibiting apoptosis [55]. However, how the oligomerization status of PKM2 is implicated in these processes, especially in cardiomyocytes, awaits further studies.

TEPP-46, a specific PKM2 tetramerization promoter, has been widely utilized and validated for its efficacy in numerous studies [23, 24, 56]. Several studies have indicated that enhancing PKM2 tetramerization is beneficial for cancer treatment [38, 57, 58], effectively prevents the progression of diabetic glomerular pathology [23] or mitigates doxorubicin-induced cardiomyocyte apoptosis [59]. Our research further substantiates that promoting PKM2 tetramerization using TEPP-46 can alleviate the progression of pulmonary arterial hypertension and right heart failure by improving mitochondrial dynamics. However, due to the involvement of dimeric or

monomeric forms of PKM2 in regulating many important cellular functions [12], potential side effects of PKM2 tetramerization therapy remains to be a significant challenge. It has been reported that promoting PKM2 tetramerization may exacerbate the progression of bleomycin induced pulmonary fibrosis [60]. Therefore, more experimental and clinical data are needed in the future to support and guide the use of PKM2 tetramerization therapy in disease treatment.

Our research also has some limitations. In vitro, PKM2 expression was not upregulated during the hypertrophy of NRVMs, which contradicts with the data observed in vivo. We believe that this inconsistency could be attributed to the naturally higher expression levels of PKM2 in fetal hearts [61]. NRVMs we utilized were derived from fetal rats, which is a commonly used cell type for cardiac research [62]. However, this did not undermine our experimental conclusions, that the disruption of PKM2 tetramers during myocardial hypertrophy affected the mitochondrial dynamics of cardiomyocytes. Secondly, we did not perform a knockdown of PKM2, for there have been numerous studies on the effects of PKM2 depletion on the cardiac dysfunction [17, 18], and our research was primarily focus on investigating the influence of altered PKM2 tetramerization on mitochondrial homeostasis in cardiomyocytes and on the progression of heart failure.

In summary, our research revealed that promoting PKM2 tetramerization could effectively improve mitochondrial network formation, and alleviate oxidative stress as well as heart failure. Targeting PKM2 tetramerization may be considered as an intervention strategy for patients with both cancer and heart disease comorbidity.

Abbreviations

PKM2	M-type pyruvate kinase 2
RVF	Right ventricular failure
SD	Sprague–Dawley
MCT	Monocrotaline
PAH	Pulmonary arterial hypertension
ATP	Adenosine triphosphate
ADP	Adenosine diphosphate
ROS	Reactive oxygen species
FAC	Fractional area change
RVSP	Right ventricular systolic pressure
RAP	Right atrial pressure
TRmax	The maximum velocity of the tricuspid regurgitant
RVA d	End-diastolic right ventricular area
RVA s	End-systolic right ventricular area
FC	Fold Change
TF	T-test
NRVMs	Neonatal rat ventricular myocytes
DMEM	Dulbecco's modified eagle medium
FBS	Fetal Bovine Serum
AVP	Arginine vasopressin
PVDF	Polyvinylidene fluoride
HRP	Horseradish peroxidase
ECL	Enhanced chemiluminescence
RT-qPCR	Quantitative real-time PCR
HE	Hematoxylin and eosin

TUNEL	Terminal deoxynucleotidyl transferase-mediated dextroxyuridine triphosphate nick-end labeling
DAPI	4',6'-Diamidino-2-phenylindole
AOPP	Advanced oxidation protein product
TEM	Transmission electron microscopy
SEM	Standard error of the mean
FDR	False discovery rate
BH	Benjamini and Hochberg
PCA	Principal component analysis
TCA	Tricarboxylic acid cycle
OXPHOS	Oxidative phosphorylation
l-OPA1	Long OPA1 forms
s-OPA1	Short OPA1 forms
PK	Pyruvate kinase
Drp1	Dynamin-Related Protein 1
OPA1	OPA1 Mitochondrial Dynamin Like GTPase
MFN2	Mitofusin 2
SERCA2	Sarcoplasmic/Endoplasmic Reticulum Calcium ATPase 2
PLN	Phospholamban
MYH6	Myosin Heavy Chain 6
MYH7	Myosin Heavy Chain 7
RYR2	Ryanodine Receptor 2
TNNT3	Troponin T3
TNNI3	Troponin I3
TNNC1	Troponin C1
BAX	BCL2 Associated X
Bcl-2	Apoptosis Regulator Bcl-2

Supplementary Information

The online version contains supplementary material available at <https://doi.org/10.1186/s12967-023-04780-6>.

Additional file 1: Figure S1. A Tricuspid regurgitation detected by echocardiography was used to represent right ventricular dysfunction and evaluate right ventricular systolic pressure (RVSP). **B** Right ventricular catheterization was used to confirm the pulmonary artery pressure. **C** Kaplan–Meier curve described the percentage of RVF rats free of tricuspid regurgitation. n = 13. **D** Principal component analysis (PCA) of quantitative proteomic data of RVF rats and control. **E** The relative mRNA level of indicated genes was determined by RT-qPCR. Results are expressed as mean ± SEM, n = 6 rats per group. **F–G** Lysates from right ventricle of control and RVF rats were analyzed by western blotting with indicated antibodies. Relative protein level was quantified and expressed as mean ± SEM, n = 4 rats in control group, n = 10 in RVF group. **H** Tricuspid regurgitation detected by echocardiography for evaluation of RVSP. **I** RVSP was measured by echocardiograph and expressed as mean ± SEM, n = 5 rats per group.

Additional file 2: Figure S2. A Rat primary cardiomyocytes were treated with 1 μM AVP for 48 h to induce hypertrophy. Mitochondrial morphology was visualized by MitoTracker-Red and OPA1 staining. Scale bar = 20 μm. **B–E** The means of area, perimeter, form factor and aspect ratio of mitochondria were quantified. Results are expressed as mean ± SEM, n = 50 cells per group. **F–I** Lysates from primary cardiomyocytes treated with AVP for indicated time were analyzed by western blotting with indicated antibodies. Relative protein level was quantified and expressed as mean ± SEM, n = 3.

Additional file 3: Table S1. Antibody list.

Additional file 4: Table S2. Primer sequences.

Additional file 5: Table S3. Total differentially expressed protein.

Additional file 6: Uncropped gels from figures.

Acknowledgements

None.

Author contributions

Conceptualization: Lizhe Guo, E Wang; Methodology: Lizhe Guo, Lu Wang, Gang Qin, Dandan Wang, Jian Qiu; Formal analysis and investigation: Junjie Zhang, Longyan Li; Writing—original draft preparation: Lizhe Guo, Jian Qiu; Writing—review and editing: Lu Wang, Gang Qin; Supervision: E Wang, Jian Qiu.

Funding

This work was supported by grants from the National Nature Science Foundation of China (grant number 82170291, 81700275, 81800058, 31972886 and 32270722) and the Hunan Provincial Natural Science Foundation of China (Grant No. 2021JJ41002, 2021JJ10074, 2022CB1004, 2021JJ31124).

Availability of data and materials

The data presented in this study are available on request from the corresponding authors.

Declarations**Ethics approval and consent to participate**

All animal experiments were carried out in accordance with the recommendations of national and international animal care and ethical guidelines and were approved by the Ethics Committee for Animal Research of Xiangya Hospital of Central South University (permit code: 2103590). The manuscript does not contain clinical studies or patient data.

Consent for publication

Yes.

Competing interests

The authors have no competing interests to declare that are relevant to the content of this article.

Author details

¹Department of Anesthesiology, Xiangya Hospital, Central South University, Changsha, China. ²Hunan Key Laboratory of Molecular Precision Medicine, Department of Neurology, Xiangya Hospital, Central South University, Changsha, China. ³National Clinical Research Center for Geriatric Disorders (Xiangya Hospital), Changsha, China. ⁴Hunan Key Laboratory of Medical Genetics, School of Life Sciences, Central South University, Changsha, Hunan, China.

Received: 4 September 2023 Accepted: 28 November 2023

Published online: 07 December 2023

References

- Simonneau G, Montani D, Celermajer DS, Denton CP, Gatzoulis MA, Krowka M, Williams PG, Souza R. Haemodynamic definitions and updated clinical classification of pulmonary hypertension. *Eur Respir J*. 2019;53(1):1801913. <https://doi.org/10.1183/13993003.01913-2018>.
- Naeije R, Richter MJ, Rubin LJ. The physiological basis of pulmonary arterial hypertension. *Eur Respir J*. 2022;59(6):2102334. <https://doi.org/10.1183/13993003.02334-2021>.
- Abid S, Marcos E, Parpaleix A, Amsellem V, Breau M, Houssaini A, Vienney N, Lefevre M, Derumeaux G, Evans S, Hubeau C, Delcroix M, Quarck R, Adnot S, Lipskaia L. CCR2/CCR5-mediated macrophage-smooth muscle cell crosstalk in pulmonary hypertension. *Eur Respir J*. 2019;54(4):1802308. <https://doi.org/10.1183/13993003.02308-2018>.
- Calvier L, Chouvarine P, Legchenko E, Hoffmann N, Geldner J, Borchert P, Jonigk D, Mozes MM, Hansmann G. PPARgamma Links BMP2 and TGFbeta1 Pathways in Vascular Smooth Muscle Cells, Regulating Cell Proliferation and Glucose Metabolism. *Cell Metab*. 2017;25(5):1118-34 e7. <https://doi.org/10.1016/j.cmet.2017.03.011>.
- Tan R, You Q, Yu D, Xiao C, Adu-Amankwaah J, Cui J, Zhang T. Novel hub genes associated with pulmonary artery remodeling in pulmonary hypertension. *Front Cardiovasc Med*. 2022;9:945854. <https://doi.org/10.3389/fcvm.2022.945854>.
- Lajoie AC, Lauziere G, Lega JC, Lacasse Y, Martin S, Simard S, Bonnet S, Provencher S. Combination therapy versus monotherapy for pulmonary arterial hypertension: a meta-analysis. *Lancet Respir Med*. 2016;4(4):291–305. [https://doi.org/10.1016/S2213-2600\(16\)00027-8](https://doi.org/10.1016/S2213-2600(16)00027-8).
- van de Veerdonk MC, Kind T, Marcus JT, Mauritz GJ, Heymans MW, Bogaard HJ, Boonstra A, Marques KM, Westerhof N, Vonk-Noordegraaf A. Progressive right ventricular dysfunction in patients with pulmonary arterial hypertension responding to therapy. *J Am Coll Cardiol*. 2011;58(24):2511–9. <https://doi.org/10.1016/j.jacc.2011.06.068>.
- Anastasiou D, Pouligiannis G, Asara JM, Boxer MB, Jiang JK, Shen M, Bellinger G, Sasaki AT, Locasale JW, Auld DS, Thomas CJ, van der Heiden MG, Cantley LC. Inhibition of pyruvate kinase M2 by reactive oxygen species contributes to cellular antioxidant responses. *Science*. 2011;334(6060):1278–83. <https://doi.org/10.1126/science.1211485>.
- Rees ML, Subramaniam J, Li Y, Hamilton DJ, Frazier OH, Taegtmeier H. A PKM2 signature in the failing heart. *Biochem Biophys Res Commun*. 2015;459(3):430–6. <https://doi.org/10.1016/j.bbrc.2015.02.122>.
- Masaki S, Hashimoto K, Kihara D, Tsuzuki C, Kataoka N, Suzuki K. The cysteine residue at 424th of pyruvate kinase M2 is crucial for tetramerization and responsiveness to oxidative stress. *Biochem Biophys Res Commun*. 2020;526(4):973–7. <https://doi.org/10.1016/j.bbrc.2020.03.182>.
- Rajala RVS. Aerobic glycolysis in the retina: functional roles of pyruvate kinase isoforms. *Front Cell Dev Biol*. 2020;8:266. <https://doi.org/10.3389/fcell.2020.00266>.
- Lee YB, Min JK, Kim JG, Cap KC, Islam R, Hossain AJ, Dogsom O, Hamza A, Mahmud S, Choi DR, Kim YS, Koh YH, Kim HA, Chung WS, Suh SW, Park JB. Multiple functions of pyruvate kinase M2 in various cell types. *J Cell Physiol*. 2022;237(1):128–48. <https://doi.org/10.1002/jcp.30536>.
- Irokawa H, Numasaki S, Kato S, Iwai K, Inose-Maruyama A, Ohdate T, Hwang GW, Toyama T, Watanabe T, Kuge S. Comprehensive analyses of the cysteine thiol oxidation of PKM2 reveal the effects of multiple oxidation on cellular oxidative stress response. *Biochem J*. 2021;478(7):1453–70. <https://doi.org/10.1042/BCJ20200897>.
- Bertero E, Maack C. Metabolic remodelling in heart failure. *Nat Rev Cardiol*. 2018;15(8):457–70. <https://doi.org/10.1038/s41569-018-0044-6>.
- Tsutsui H, Kinugawa S, Matsushima S. Oxidative stress and heart failure. *Am J Physiol Heart Circ Physiol*. 2011;301(6):H2181–90. <https://doi.org/10.1152/ajpheart.00554.2011>.
- Magadum A, Singh N, Kurian AA, Munir I, Mehmood T, Brown K, Sharkar MTK, Chepurko E, Sassi Y, Oh JG, Lee P, Santos CXC, Gaziel-Sovran A, Zhang G, Cai CL, Kho C, Mayr M, Shah AM, Hajjar RJ, Zangi L. Pkm2 regulates cardiomyocyte cell cycle and promotes cardiac regeneration. *Circulation*. 2020;141(15):1249–65. <https://doi.org/10.1161/CIRCULATIONAHA.119.043067>.
- Hauck L, Dadson K, Chauhan S, Grothe D, Billia F. Inhibiting the Pkm2/b-catenin axis drives in vivo replication of adult cardiomyocytes following experimental MI. *Cell Death Differ*. 2021;28(4):1398–417. <https://doi.org/10.1038/s41418-020-00669-9>.
- Ni L, Lin B, Hu L, Zhang R, Fu F, Shen M, Yang J, Shi D. Pyruvate kinase M2 protects heart from pressure overload-induced heart failure by phosphorylating RAC1. *J Am Heart Assoc*. 2022;11(11):e024854. <https://doi.org/10.1161/JAHA.121.024854>.
- Shimauchi T, Boucherat O, Yokokawa T, Grobs Y, Wu W, Orcholski M, Martineau S, Omura J, Tremblay E, Shimauchi K, Nadeau V, Breuils-Bonnet S, Paulin R, Potus F, Provencher S, Bonnet S. PARP1-PKM2 axis mediates right ventricular failure associated with pulmonary arterial hypertension. *JACC Basic Transl Sci*. 2022;7(4):384–403. <https://doi.org/10.1016/j.jacbs.2022.01.005>.
- Guo L, Qin G, Cao Y, Yang Y, Dai S, Wang L, Wang E. Regulation of the immune microenvironment by an NLRP3 inhibitor contributes to attenuation of acute right ventricular failure in rats with pulmonary arterial hypertension. *J Inflamm Res*. 2021;14:5699–711. <https://doi.org/10.2147/JIR.S336964>.
- Tian S, Zhan D, Yu Y, Wang Y, Liu M, Tan S, Li Y, Song L, Qin Z, Li X, Liu Y, Li Y, Ji S, Wang S. Proteomic Massive Analysis and Quality Control Consortium, Zheng Y, He F, Qin J, Ding C. Quartet protein reference materials and datasets for multi-platform assessment of label-free proteomics. *Genome Biol*. 2023;24(1):202. <https://doi.org/10.1186/s13059-023-03048-y>.
- Benjamini Y, Hochberg Y. Controlling the false discovery rate: a practical and powerful approach to multiple testing. *J Roy Stat Soc Ser B Methodol*. 2018;57(1):289–300. <https://doi.org/10.1111/j.2517-6161.1995.tb02031.x>.

23. Qi W, Keenan HA, Li Q, Ishikado A, Kann T, Sadowski T, Yorek MA, Wu IH, Lockhart S, Copeley LJ, Pfenninger A, Liew CW, Qiang G, Burkart AM, Hastings S, Pober D, Cahill C, Niewczasz MA, Israelsen WJ, Tinsley L, Stillman IE, Amenta PS, Feener EP, van der Heiden MG, Stanton RC, King GL. Pyruvate kinase M2 activation may protect against the progression of diabetic glomerular pathology and mitochondrial dysfunction. *Nat Med*. 2017;23(6):753–62. <https://doi.org/10.1038/nm.4328>.
24. Gao S, Li X, Jiang Q, Liang Q, Zhang F, Li S, Zhang R, Luan J, Zhu J, Gu X, Xiao T, Huang H, Chen S, Ning W, Yang G, Yang C, Zhou H. PKM2 promotes pulmonary fibrosis by stabilizing TGF- β 1 receptor I and enhancing TGF- β 1 signaling. *Sci Adv*. 2022;8(38):eabo0987. <https://doi.org/10.1126/sciadv.abo0987>.
25. Hsu CC, Zhang X, Wang G, Zhang W, Cai Z, Pan BS, Gu H, Xu C, Jin G, Xu X, Manne RK, Jin Y, Yan W, Shao J, Chen T, Lin E, Ketkar A, Eoff R, Xu ZG, Chen ZZ, Li HY, Lin HK. Inositol serves as a natural inhibitor of mitochondrial fission by directly targeting AMPK. *Mol Cell*. 2021;81(18):3803–19 e7. <https://doi.org/10.1016/j.molcel.2021.08.025>.
26. Dagda RK, Cherra SJ, Kulich SM, Tandon A, Park D, Chu CT. Loss of PINK1 function promotes mitophagy through effects on oxidative stress and mitochondrial fission. *J Biol Chem*. 2009;284(20):13843–55. <https://doi.org/10.1074/jbc.M808515200>.
27. Legland D, Arganda-Carreras I, Andrey P. MorphoLibJ: integrated library and plugins for mathematical morphology with ImageJ. *Bioinformatics*. 2016;32(22):3532–4. <https://doi.org/10.1093/bioinformatics/btw413>.
28. Gao H, Cheng Y, Zong L, Huang L, Qiao C, Li W, Gong B, Hu J, Liu H, Wang X, Zhao C. Aspirin attenuates monocrotaline-induced pulmonary arterial hypertension in rats by suppressing the ERK/MAPK pathway. *Clin Exp Hypertens*. 2017;39(1):34–41. <https://doi.org/10.1080/10641963.2016.1210620>.
29. Li Q, Wang J, Zhu X, Zeng Z, Wu X, Xu Y, Xie J, Yu J. Dihydropyridine prevents monocrotaline-induced pulmonary arterial hypertension in rats. *Biomed Pharmacother*. 2017;96:825–33. <https://doi.org/10.1016/j.biopha.2017.10.007>.
30. Carlson CR, Aronsen JM, Bergan-Dahl A, Moutty MC, Lunde M, Lunde PK, Jarstadmarken H, Wanichawan P, Pereira L, Kolstad TRS, Dalhus B, Subramanian H, Hille S, Christensen G, Muller OJ, Nikolaev V, Bers DM, Sjaastad I, Shen X, Louch WE, Klussmann E, Sejersted OM. AKAP18delta anchors and regulates CaMKII activity at phospholamban-SERCA2 and RYR. *Circ Res*. 2022;130(1):27–44. <https://doi.org/10.1161/CIRCRESAHA.120.317976>.
31. Van Spaendonck-Zwarts KY, Posafalvi A, van den Berg MP, Hilfiker-Kleiner D, Bollen IA, Sliwa K, Alders M, Almomani R, van Langen IM, van der Meer P, Sinke RJ, van der Velden J, van Veldhuisen DJ, van Tintelen JP, Jongbloed JD. Titin gene mutations are common in families with both peripartum cardiomyopathy and dilated cardiomyopathy. *Eur Heart J*. 2014;35(32):2165–73. <https://doi.org/10.1093/eurheartj/ehu050>.
32. Vigil-Garcia M, Demkes CJ, Eding JEC, Versteeg D, de Ruiter H, Perini I, Kooijman L, Gladka MM, Asselbergs FW, Vink A, Harakalova M, Bossu A, van Veen TAB, Boogerd CJ, van Rooij E. Gene expression profiling of hypertrophic cardiomyocytes identifies new players in pathological remodelling. *Cardiovasc Res*. 2021;117(6):1532–45. <https://doi.org/10.1093/cvr/cvaa233>.
33. Sawaki D, Czibik G, Pini M, Ternacle J, Suffee N, Mercedes R, Marcellin G, Surenaud M, Marcos E, Gual P, Clement K, Hue S, Adnot S, Hatem SN, Tsuchimochi I, Yoshimitsu T, Henegar C, Derumeaux G. Visceral adipose tissue drives cardiac aging through modulation of fibroblast senescence by osteopontin production. *Circulation*. 2018;138(8):809–22. <https://doi.org/10.1161/CIRCULATIONAHA.117.031358>.
34. Mackinnon AC, Gibbons MA, Farnworth SL, Leffler H, Nilsson UJ, Delaine T, Simpson AJ, Forbes SJ, Hirani N, Gaudie J, Sethi T. Regulation of transforming growth factor- β 1-driven lung fibrosis by galectin-3. *Am J Respir Crit Care Med*. 2012;185(5):537–46. <https://doi.org/10.1164/rccm.201106-0965OC>.
35. Liu Z, Wang L, Welch JD, Ma H, Zhou Y, Vaseghi HR, Yu S, Wall JB, Alimohamadi S, Zheng M, Yin C, Shen W, Prins JF, Liu J, Qian L. Single-cell transcriptomics reconstructs fate conversion from fibroblast to cardiomyocyte. *Nature*. 2017;551(7678):100–4. <https://doi.org/10.1038/nature24454>.
36. Zhao J, Lei Y, Yang Y, Gao H, Gai Z, Li X. Metoprolol alleviates arginine vasopressin-induced cardiomyocyte hypertrophy by upregulating the AKT1-SERCA2 cascade in H9C2 cells. *Cell Biosci*. 2020;10:72. <https://doi.org/10.1186/s13578-020-00434-y>.
37. Chen S, Li Y, Fu S, Li Y, Wang C, Sun P, Li H, Tian J, Du GQ. Melatonin alleviates arginine vasopressin-induced cardiomyocyte apoptosis via increasing Mst1-Nrf2 pathway activity to reduce oxidative stress. *Biochem Pharmacol*. 2022;206:115265. <https://doi.org/10.1016/j.bcp.2022.115265>.
38. Anastasiou D, Yu Y, Israelsen WJ, Jiang JK, Boxer MB, Hong BS, Tempel W, Dimov S, Shen M, Jha A, Yang H, Mattaini KR, Metallo CM, Fiske BP, Courtney KD, Malstrom S, Khan TM, Kung C, Skoumbouris AP, Veith H, Southall N, Walsh MJ, Brimacombe KR, Leister W, Lunt SY, Johnson ZR, Yen KE, Kunii K, Davidson SM, Christofk HR, Austin CP, Inglesse J, Harris MH, Asara JM, Stephanopoulos G, Salituro FG, Jin S, Dang L, Auld DS, Park HW, Cantley LC, Thomas CJ, van der Heiden MG. Pyruvate kinase M2 activators promote tetramer formation and suppress tumorigenesis. *Nat Chem Biol*. 2012;8(10):839–47. <https://doi.org/10.1038/nchembio.1060>.
39. Legchenko E, Chouvarine P, Borchert P, Fernandez-Gonzalez A, Snay E, Meier M, Maegel L, Mitsialis SA, Rog-Zielinska EA, Kourembanas S, Jonigk D, Hansmann G. PPAR γ agonist pioglitazone reverses pulmonary hypertension and prevents right heart failure via fatty acid oxidation. *Sci Transl Med*. 2018;10(438):eaao0303. <https://doi.org/10.1126/scitranslmed.aao0303>.
40. Wernig F, Xu Q. Mechanical stress-induced apoptosis in the cardiovascular system. *Prog Biophys Mol Biol*. 2002;78(2–3):105–37. [https://doi.org/10.1016/s0079-6107\(02\)00008-1](https://doi.org/10.1016/s0079-6107(02)00008-1).
41. Zungu-Edmondson M, Shults NV, Wong CM, Suzuki YJ. Modulators of right ventricular apoptosis and contractility in a rat model of pulmonary hypertension. *Cardiovasc Res*. 2016;110(1):30–9. <https://doi.org/10.1093/cvr/cvw014>.
42. Nomura S, Satoh M, Fujita T, Higo T, Sumida T, Ko T, Yamaguchi T, Tobita T, Naito AT, Ito M, Fujita K, Harada M, Toko H, Kobayashi Y, Ito K, Takimoto E, Akazawa H, Morita H, Aburatani H, Komuro I. Cardiomyocyte gene programs encoding morphological and functional signatures in cardiac hypertrophy and failure. *Nat Commun*. 2018;9(1):4435. <https://doi.org/10.1038/s41467-018-06639-7>.
43. Marin-Garcia J, Akhmedov AT, Moe GW. Mitochondria in heart failure: the emerging role of mitochondrial dynamics. *Heart Fail Rev*. 2013;18(4):439–56. <https://doi.org/10.1007/s10741-012-9330-2>.
44. Aimo A, Borrelli C, Vergaro G, Piepoli MF, Caterina AR, Mirizzi G, Valleggi A, Raglianti V, Passino C, Emdin M, Giannoni A. Targeting mitochondrial dysfunction in chronic heart failure: current evidence and potential approaches. *Curr Pharm Des*. 2016;22(31):4807–22. <https://doi.org/10.2174/1381612822666160701075027>.
45. Lorenzana-Carrillo MA, Gopal K, Byrne NJ, Tejay S, Saleme B, Das SK, Zhang Y, Haromy A, Eaton F, MendiolaPla M, Bowles DE, Dyck JRB, Ussher JR, Michelakis ED, Sutendra G. TRIM35-mediated degradation of nuclear PKM2 destabilizes GATA4/6 and induces P53 in cardiomyocytes to promote heart failure. *Sci Transl Med*. 2022;14(669):eabm3565. <https://doi.org/10.1126/scitranslmed.abm3565>.
46. Tang Y, Feng M, Su Y, Ma T, Zhang H, Wu H, Wang X, Shi S, Zhang Y, Xu Y, Hu S, Wei K, Xu D. Jmjd4 facilitates Pkm2 degradation in cardiomyocytes and is protective against dilated cardiomyopathy. *Circulation*. 2023;147(22):1684–704. <https://doi.org/10.1161/CIRCULATIONAHA.123.064121>.
47. Hitosugi T, Kang S, van der Heiden MG, Chung TW, Elf S, Lythgoe K, Dong S, Lonial S, Wang X, Chen GZ, Xie J, Gu TL, Polakiewicz RD, Roesel JL, Boggon TJ, Khuri FR, Gilliland DG, Cantley LC, Kaufman J, CHEN J. Tyrosine phosphorylation inhibits PKM2 to promote the Warburg effect and tumor growth. *Sci Signal*. 2009;2(97):73. <https://doi.org/10.1126/scisignal.2000431>.
48. Wu C, Zhang Z, Zhang W, Liu X. Mitochondrial dysfunction and mitochondrial therapies in heart failure. *Pharmacol Res*. 2022;175:106038. <https://doi.org/10.1016/j.phrs.2021.106038>.
49. Noone J, O’Gorman DJ, Kenny HC. OPA1 regulation of mitochondrial dynamics in skeletal and cardiac muscle. *Trends Endocrinol Metab*. 2022;33(10):710–21. <https://doi.org/10.1016/j.tem.2022.07.003>.
50. Xiong PY, Tian L, Dunham-Snary KJ, Chen KH, Mewburn JD, Neuber-Hess M, Martin A, Dasgupta A, Potus F, Archer SL. Biventricular increases in mitochondrial fission mediator (MiD51) and proglycolytic pyruvate kinase (PKM2) isoform in experimental group 2 pulmonary hypertension-novel mitochondrial abnormalities. *Front Cardiovasc Med*. 2018;5:195. <https://doi.org/10.3389/fcvm.2018.00195>.
51. Tian L, Neuber-Hess M, Mewburn J, Dasgupta A, Dunham-Snary K, Wu D, Chen KH, Hong Z, Sharp WW, Kutty S, Archer SL. Ischemia-induced Drp1

- and Fis1-mediated mitochondrial fission and right ventricular dysfunction in pulmonary hypertension. *J Mol Med*. 2017;95(4):381–93. <https://doi.org/10.1007/s00109-017-1522-8>.
52. Lozhkin A, Vendrov AE, Ramos-Mondragon R, Canugovi C, Stevenson MD, Herron TJ, Hummel SL, Figueroa CA, Bowles DE, Isom LL, Runge MS, Madamanchi NR. Mitochondrial oxidative stress contributes to diastolic dysfunction through impaired mitochondrial dynamics. *Redox Biol*. 2022;57: 102474. <https://doi.org/10.1016/j.redox.2022.102474>.
 53. Wai T, Garcia-Prieto J, Baker MJ, Merkwirth C, Benit P, Rustin P, Ruperez FJ, Barbas C, Ibanez B, Langer T. Imbalanced OPA1 processing and mitochondrial fragmentation cause heart failure in mice. *Science*. 2015;350(6265):aad0116. <https://doi.org/10.1126/science.aad0116>.
 54. Li T, Han J, Jia L, Hu X, Chen L, Wang Y. PKM2 coordinates glycolysis with mitochondrial fusion and oxidative phosphorylation. *Protein Cell*. 2019;10(8):583–94. <https://doi.org/10.1007/s13238-019-0618-z>.
 55. Liang J, Cao R, Wang X, Zhang Y, Wang P, Gao H, Li C, Yang F, Zeng R, Wei P, Li D, Li W, Yang W. Mitochondrial PKM2 regulates oxidative stress-induced apoptosis by stabilizing Bcl2. *Cell Res*. 2017;27(3):329–51. <https://doi.org/10.1038/cr.2016.159>.
 56. Liu F, Ma M, Gao A, Ma F, Ma G, Liu P, Jia C, Wang Y, Donahue K, Zhang S, Ong IM, Keles S, Li L, Xu W. PKM2-TMEM33 axis regulates lipid homeostasis in cancer cells by controlling SCAP stability. *EMBO J*. 2021;40(22): e108065. <https://doi.org/10.15252/embj.2021108065>.
 57. Apostolidi M, Vathiotis IA, Muthusamy V, Gaule P, Gassaway BM, Rimm DL, Rinehart J. Targeting pyruvate kinase M2 phosphorylation reverses aggressive cancer Phenotypes. *Cancer Res*. 2021;81(16):4346–59. <https://doi.org/10.1158/0008-5472.Can-20-4190>.
 58. Mohammad GH, Vassileva V, Acedo P, Olde Damink SWM, Malago M, Dhar DK, Pereira SP. Targeting pyruvate kinase M2 and lactate dehydrogenase A is an effective combination strategy for the treatment of pancreatic cancer. *Cancers*. 2019;11(9):1372. <https://doi.org/10.3390/cancers11091372>.
 59. Saleme B, Gurtu V, Zhang Y, Kinnaird A, Boukouris AE, Gopal K, Ussher JR, Sutendra G. Tissue-specific regulation of p53 by PKM2 is redox dependent and provides a therapeutic target for anthracycline-induced cardiotoxicity. *Sci Transl Med*. 2019;11(478):aau8866. <https://doi.org/10.1126/scitranslmed.aau8866>.
 60. Gao S, Li X, Jiang Q, Liang Q, Zhang F, Li S, Zhang R, Luan J, Zhu J, Gu X, Xiao T, Huang H, Chen S, Ning W, Yang G, Yang C, Zhou H. PKM2 promotes pulmonary fibrosis by stabilizing TGF- β 1 receptor I and enhancing TGF- β 1 signaling. *Sci Adv*. 2022;8(38):abo0987. <https://doi.org/10.1126/sciadv.abo0987>.
 61. Rihan M, Sharma SS. Role of pyruvate kinase M2 (PKM2) in cardiovascular diseases. *J Cardiovasc Transl Res*. 2023;16(2):382–402. <https://doi.org/10.1007/s12265-022-10321-1>.
 62. Wang X, Zhang G, Dasgupta S, Niewold EL, Li C, Li Q, Luo X, Tan L, Ferdous A, Lorenzi PL, Rothermel BA, Gillette TG, Adams CM, Scherer PE, Hill JA, Wang ZV. ATF4 protects the heart from failure by antagonizing oxidative stress. *Circ Res*. 2022;131(1):91–105. <https://doi.org/10.1161/circresaha.122.321050>.

Publisher's Note

Springer Nature remains neutral with regard to jurisdictional claims in published maps and institutional affiliations.

Ready to submit your research? Choose BMC and benefit from:

- fast, convenient online submission
- thorough peer review by experienced researchers in your field
- rapid publication on acceptance
- support for research data, including large and complex data types
- gold Open Access which fosters wider collaboration and increased citations
- maximum visibility for your research: over 100M website views per year

At BMC, research is always in progress.

Learn more biomedcentral.com/submissions

